Track structure characterization and its link to radiobiology

V. Conte [a, *], A. Selva [a, b], P. Colautti [a], G. Hilgers [c], H. Rabus [c]

[a] INFN - Legnaro National Laboratories, Viale dell'Università 2, I-35020 Legnaro, Italy
[b] Department of Physics and Astronomy, University of Padova, Via Marzolo 8, I-35131 Padova, Italy
[c] Physikalisch-Technische Bundesanstalt (PTB), Braunschweig, Germany

HIGHLIGHTS

- Track structure measurements at nanometre level performed with two detectors.
- Cumulative probabilities F_k of cluster sizes $\nu \geq k$ derived from measurements.
- The relation of F_k to radiobiology is presented and discussed.

ARTICLE INFO

Keywords:
Nanodosimetry
Radiation quality
Track structure

ABSTRACT

Within the Italian project MITRA (**MI**crodosimetry and **TRA**ck structure), funded by the Italian **I**stituto **N**azionale di **F**isica **N**ucleare (INFN), and the EMRP Joint Research Project "BioQuaRT" (**Bio**logically Weighted **Qua**ntities in **R**adio**t**herapy), experiments have been carried out at the Tandem–Alpi accelerator facility of Legnaro National Laboratories (LNL), in which the frequency distribution of the number of ionisations produced by proton and carbon ion beams of given energy was measured with the PTB Ion Counter and the LNL StarTrack Counter. Descriptors of the track structure can be derived from these distribution; in particular, the first moment M_1, representing the mean number of ionisations produced in the target volume, and the cumulative probabilities F_k of measuring cluster sizes $\nu \geq k$.

Experimental radiobiological data have been compared with nanodosimetric quantities derived from measured ionisation-cluster size distributions. It was found that the cumulative probabilities F_k as a function of M_1 behave in the same way as the inactivation cross sections as a function of LET, first increasing with increasing values of M_1 and then showing a saturation effect.

A comparison of F_k and radiobiological quantities is presented and discussed.

1. Introduction

It is largely recognised that the absorbed dose is a quantity that is not adequate to describe the biological effects of ionising radiation. Indeed, the absorbed dose required to produce a given biological effect depends on the type of radiation field. It also varies between ionising particles of same type if they have different energies. Therefore, the biological effectiveness of radiation depends on radiation quality, which is defined by the particle type and energy.

As a consequence, in the context of radiation protection as well as in radiation therapy applications, the assessment of the absorbed dose only is not sufficient. In addition, the relative biological effectiveness (RBE) of the radiation has also to be taken into account. Generally, the RBE of a given radiation is evaluated with time-consuming radiobiological experiments. In the context of radiation therapy, these experiments can be performed in order to periodically verify the predictions of the applied treatment–planning systems. As measurements of cell survival generally take several weeks, they are too slow to be used as a predictive assay for the clinical response of irradiated cancers. Experimental nanodosimetry offers an alternative procedure to estimate the biological effectiveness of ionising radiation from a concept of radiation quality that builds on measurable characteristics of the particle track structure at the nanometre scale. The properties of particle track structure are strongly related to the stochastic nature of particle interaction. In nanodosimetry, the stochastics of the so-called ionisation cluster size (ICS), i.e. the number of ionisations

* Corresponding author. INFN – Legnaro National Laboratories, Viale dell'Università 2, I-35020 Legnaro, PD, Italy.
E-mail address: conte@lnl.infn.it (V. Conte).

produced inside a specified target volume by the interaction of single ion tracks is investigated experimentally. The measurement assesses the relative frequencies $P_\nu(Q,V)$ which are estimators of the probabilities for an ionisation cluster of size ν being produced by ionising particles of radiation quality Q (charge state and velocity) in a specific target volume V.

Three different types of nanodosimeters have been developed to date (Conte et al., 2012; Garty et al., 2002; Pszona et al., 2000); all of them are gas–based detectors, in which a millimetre-sized volume is filled with a gas at low density, to reproduce the same stochastics of ionising interactions as in a nanometre-sized volume of liquid water (Grosswendt et al., 2004). The three devices differ in type and density of the target gas, in the geometry and size of the sensitive volume, and they have different response functions. Two of these devices detect the ions produced in the ionisation processes, the other one detects the electrons.

In the framework of the European Joint Research Project BioQuaRT (Biologically Weighted Quantities in Radiotherapy) and of the Italian project MITRA (MIcrodosimetry and TRAck structure), funded by INFN, experiments have been carried out at the Tandem-Alpi accelerator facility of the LNL. Carbon ion and proton beams of different radiation quality were measured with the LNL StarTrack Counter and with the PTB Ion Counter.

2. Instruments and methods

2.1. Experimental setup

The measurements discussed in the present paper were carried out with two nanodosimeters, whose characteristics are substantially different. The LNL Startrack Counter measures the ionisations by counting the electrons set free in the ionisation process. The counter consists of a sensitive volume (*SV*) and a single electron counter. The latter is made of a long cylindrical drift column and an electron multiplier, based on a multi–step avalanche chamber (MSAC). The sensitive volume is defined through the static electric field inside several miniaturized circular electrodes delineating a right cylinder 3.7 mm in diameter and height. Electrons generated inside the *SV* are transferred into the drift column, where they diffuse and finally get into the MSAC at different times, thus allowing to separately count the electrons which belong to the initial cluster. The average electron detection efficiency is about 20%, which means that, on average, 20 out of 100 initial electrons generated in the *SV* are counted at the MSAC and recorded by the acquisition system. The electron counting starts when the primary particle interacts with a solid state detector placed at the end of the beam line.

The sensitive volume is filled with propane gas at a pressure between 200 Pa and 300 Pa. At 300 Pa the mass per area of the volume diameter is about 2 μg cm^{-2}, which corresponds to a length of 20 nm when scaled to a density of 1 g cm^{-3}. A more detailed description can be found in (Conte et al., 2012).

On the other side, the PTB Ion Counter detects the positive ions produced by ionisation events. The detector consists of a low–pressure interaction chamber containing an electrode system shaped like a plane parallel capacitor for extracting ions from the interaction chamber, an evacuated acceleration stage with an ion counter at its end, and a primary particle detector.

An ion which enters into the interaction region traversing it parallel to the capacitor electrodes, is registered at the capacitors end in a semiconductor detector that acts as a trigger. The ionised gas molecules generated by the primary particle (and by all its secondary electrons) along its track drift toward the lower capacitor electrode, because of the electrical field applied across the plane parallel plate capacitor. The ions passing through the extraction aperture in the lower capacitor electrode are guided through the acceleration stage for being detected by the ion counter. The electric field strength between the capacitor electrodes is selected in such a way that neither the already ionised gas molecules nor the electrons arising from these ionisations can generate additional ions. The shape and size of the target volume are defined by the spatial distribution of the collection efficiency of the generated ions, which is primarily determined by the electric field strength inside the plane parallel capacitor as well as the filling gas and its pressure. The interaction chamber is filled with a low density gas, for instance propane or nitrogen. There is an upper limit for the gas pressure, related to the efficiency of the differential pumping system, which is about 150 Pa for propane. To give an idea of the size of the target volume of the PTB Counter, with propane at 120 Pa the mass per area along 1 mm, corresponding to the diameter of the entrance aperture connecting the interaction chamber to the detection zone, is about 0.2 μg cm^{-2}. This corresponds to a length of 2 nm when scaled to a density of 1 g cm^{-3}. More details are given in (Garty et al., 2002).

2.2. Nanodosimetric measurements

Measurements with protons and ^{12}C-ions at several specific energies between 3.5 MeV/u and 20 MeV/u were performed with the two devices at the Tandem-Alpi accelerator complex of the INFN-Legnaro National Laboratories. The Startrack counter was filled with propane gas at the pressures of 200 Pa and 300 Pa and the Ion Counter was filled either with propane or with nitrogen at pressures of 75 Pa and 120 Pa, respectively. To give an example of the results, Fig. 1 shows the ionisation-cluster size distributions $P_\nu(Q,V)$ for 96 MeV ^{12}C-ions passing centrally through the target volumes of the PTB Ion Counter filled with propane at 120 Pa (squared symbols in the figure) and of the LNL Startrack Counter filled with propane at 300 Pa (circles in the figure).

The shape of the two distributions is similar, apart from the decrease at cluster sizes $\nu > 15$ which is steeper in the case of the Startrack Counter as compared to the Ion Counter. The different slopes beyond the peaks of the distributions reflect the different response functions of the detectors, in particular the limited efficiency of the Startrack Counter at large cluster sizes, as already described and discussed in (Conte et al., 2012). It is also immediately evident from Fig. 1 that the distributions measured with the

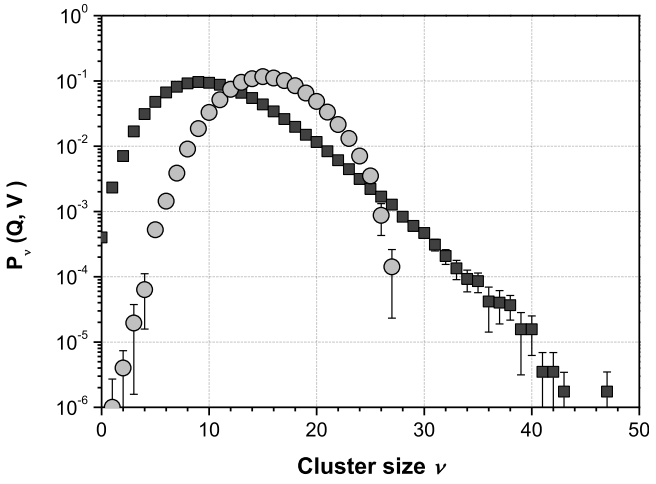

Fig. 1. Ionisation-cluster size distributions $P_\nu(Q,V)$ for 96 MeV ^{12}C-ions, measured with the Startrack Counter (light grey circles) and with the Ion Counter (dark grey squares) for particles traversing the target volumes at their centres. Only statistical uncertainties are indicated.

Startrack Counter are peaked at cluster sizes larger than those measured by the Ion Counter. This discrepancy is due to a combined effect of the different target sizes and average detection efficiencies.

3. Results and discussion

3.1. The cumulative relative frequencies F_k

Basing on the measured distribution $P_\nu(Q,V)$ of relative frequencies, the mean ionisation yield of ionising particles in the target volume is given by the first moment $M_1(Q,V)$ of the distribution:

$$M_1(Q,V) = \sum_{\nu=1}^{\infty} \nu \cdot P_\nu(Q,V) \tag{1}$$

The cumulative probability of forming ionisation-cluster sizes $\nu \geq k$ is given by the cumulative distribution functions defined by Equation (2).

$$F_k(Q,V) = \sum_{\nu=k}^{\infty} P_\nu(Q,V) \tag{2}$$

$F_1(Q,V)$ represents the probability of cluster-size formation with $\nu \geq 1$, i.e. the probability for an ionising particle to create at least one ionisation in the volume V. From the point of view of radiobiology, $F_2(Q,V)$, i.e. the probability of generating at least two ionisations is of primary importance, since it might be useful for describing the formation of double-strand breaks in the DNA.

Fig. 2 shows a synopsis of the $M_1(Q,V)$ and $F_2(Q,V)$ values derived from all measured ionisation-cluster size distributions. Each data point represents a measurement for a specific radiation quality Q with a particular nanodosimeter simulating a given nanometre-sized target volume V. Published data for 4.6 MeV alpha particles measured with the JET Counter at different site sizes (Pszona et al., 2006) are also plotted (dark–grey triangles). The horizontal axis is the mean ionisation yield M_1, i.e. the mean number of ionisations that is obtained for the combination of radiation quality and site size.

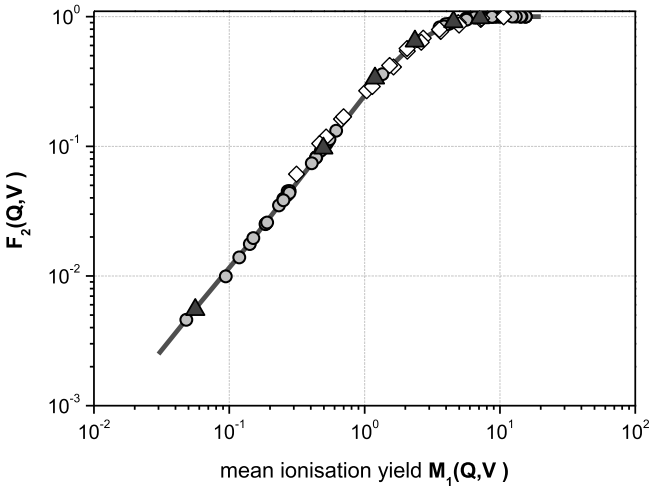

Fig. 2. The cumulative relative frequency $F_2(Q, V)$ for ionisation-cluster size equal or higher than two against the mean ionisation yield M_1. Measurements were performed for several radiation qualities, with the Startrack counter (grey circles) and the Ion Counter (white diamonds). Published data for 4.6 MeV alpha particles (Pszona et al., 2006) are also plotted (dark–grey triangles). The type A standard uncertainties, evaluated according to GUM definitions [*Guide to the expression of uncertainty in measurement*, JCGM 100 (2008)] fall within symbols. The grey line is plotted as a guide to the eye.

When plotted versus the mean ionisation yield M_1, the F_2 values turn out to be located almost on the same curve. This indicates that F_2 is approximately a unique function of M_1, independent of the simulated site size and also of the detector and its particularities. In addition, this function saturates at large M_1, similarly to the behaviour of inactivation cross sections with increasing linear energy transfer (LET). The same results were also obtained for F_1 and F_3.

From the physical point of view, the almost unique curves found when plotting the sum distributions $F_1(Q,D)$, $F_2(Q,D)$ and $F_3(Q,D)$ as a function of $M_1(Q,D)$ can be explained by the following facts: (i) the probability of k primary ionisation is described by an ordinary Poisson process; (ii) each primary ionisation comes with an associated random variable that represents the contribution of the δ-electron; (iii) these variables are independent and identically distributed, and independent of the underlying Poisson process; (iv) the contribution of each δ-electron is almost invariant with radiation quality; (v) the contribution of each δ-electron depends on site size but with a minor influence on the functional dependency of F_k on M_1, at least for $k = 1, 2, 3$.

Based on the first three facts, the overall probability $P_\nu(Q,V)$ of ionisation-cluster size ν can be described as a Poisson-distributed random sum (the k primary ionisations) of random variables, i.e. a compound Poisson-process.

Considering that the quantities F_k are intuitively related to the complexity of DNA damage, the correlation of F_k with the inactivation cross sections was investigated afterwards.

3.2. Inactivation cross sections

Published data on inactivation of V79 cells irradiated with proton (Belli et al., 1998; Folkard et al., 1996; Goodhead et al., 1992; Perris et al., 1986; Prise et al., 1990) and carbon ion beams (Belli et al., 2008; Furusawa et al., 2000; Weyrather et al., 1999) have been analysed. The relationship between the cell surviving fraction (i.e. the fraction of irradiated cells preserving their reproductive capability) and the absorbed dose is generally described by a cell survival curve. This curve shows the surviving fraction on a logarithmic scale on the ordinate against the absorbed dose on a linear scale. To interpolate radiobiological data, the cell survival curve is generally described by the linear-quadratic model:

$$S(D) = \exp\left(-\alpha D - \beta D^2\right) \tag{3}$$

where $S(D)$ is the fraction of cells surviving a dose D, α is a constant describing the initial slope of the cell survival curve, and β is a constant describing the quadratic component of cell killing.

Since nanodosimetric measurements are based on individual particle crossing, a fluence related parameter should be defined for describing charged particle effects. The inactivation cross section σ_l is usually assessed from the slope of the survival curves, according to the following equation (Belloni et al., 2002):

$$\sigma_l \Phi_l = s_l D_l \tag{4}$$

where the subscript l indicates the survival level, Φ_l is the particle fluence corresponding to the dose D_l and s_l is the slope of the survival curve in the semi–logarithmic plot at dose $D = D_l$. According to equation (3):

$$s_l = -\left.\frac{\mathrm{d}\ln S(D)}{\mathrm{d}D}\right|_{D=D_l} = \alpha + 2\beta D_l \tag{5}$$

The equation for the tangent at $S(D_l) = l$ is:

$$S(D) = l \cdot \exp[-s_l \cdot (D - D_l)] \quad (6)$$

By using again equation (3) to express D_l in terms of α, β and l, and introducing this in equation (5), s_l can also be expressed in terms of α, β and l as:

$$s_l = \sqrt{\alpha^2 - 4\beta \ln(l)} \quad (7)$$

Since the dose $D_l \propto \Phi_l \cdot LET/\rho$, from equations (4) and (7), the cross section σ_l can be expressed in terms of α, β and l as:

$$\sigma_l = \frac{k}{\rho} LET \sqrt{\alpha^2 - 4\beta \ln(l)} \quad (8)$$

where ρ is the density of the irradiated matter and $k = 0.1602$ if LET is given in keV·μm^{-1}, ρ in g·cm^{-3}, α in Gy^{-1}, β in Gy^{-2} and σ in μm^2. In this work two end points were considered, at $l = 1$ and $l = 0.05$, to calculate σ_α and $\sigma_{5\%}$.

A synopsis of inactivation cross sections for several V79 cell survival curves, calculated with equation (8), is shown in Fig. 3 against the LET of the incident particle.

By comparing Figs. 2 and 3, the similarity in shape between the physical quantity F_2 plotted against M_1 and the inactivation cross sections $\sigma_{5\%}$ plotted against LET appears clearly evident. Notably, in both figures the horizontal and the vertical axes span four and three orders of magnitude, respectively. In order to compare the physical and the biological data, pairwise measurements should be considered for the same radiation field, characterized either by LET or by M_1. Unfortunately the LET is not really known for practical mixed radiation fields and is also not easily measurable.

On the other hand, the mean ionisation cluster size $M_1(Q,V)$ is a natural parameter of ionisation cluster-size distributions and is measurable also in mixed radiation fields. Unfortunately, nanodosimetric measurements are not yet available for all the radiation qualities considered in radiobiological data from the literature. Therefore, a direct connection cannot yet be demonstrated between each inactivation cross section $\sigma_{5\%}$ and an experimentally measured mean ionisation yield M_1 and cumulative frequency F_k. However, as a first approximation it can be assumed that, for a given site size, $M_1(Q,V)$ is roughly proportional to the LET of the incident primary particles. In particular, the ratio of M_1 to LET was found to be approximately the same for protons and for carbon ions with specific energies ranging from 5 MeV/u to 20 MeV/u, for a specific target size. Therefore, the dependence of the ratio M_1/LET on the particle type and velocity plays a minor role and can be disregarded herein.

However, for a more accurate analysis, one should take into account that $M_1(Q,V)$ depends on the particle type and velocity, so that particles of the same LET can give rise to different M_1.

In view of the approximate proportionality between LET and M_1 for a given site size, it is possible to compare inactivation cross sections and nanodosimetric quantities as shown in Fig. 4. The vertical axis represents both $\sigma_{5\%}$, the inactivation cross section of V79 cells at 5% survival level (coloured symbols) and the physical quantities F_1, F_2 and F_3, multiplied by a constant proportionality coefficient $C_{5\%} = 65$ μm^2 (black and grey symbols and lines). The inactivation cross sections refer to the upper horizontal axis that is the particles' LET. The physical quantities F_k refer to the lower horizontal axis which is the mean ionisation yield M_1. Notably both LET and M_1 in the upper and lower axes span the same relative range of four orders of magnitude.

At first glance there is an almost perfect overlap of the biological and the physical data F_2. In order to optimize this overlap, the upper horizontal axis has been shifted in such a way that the LET of 100 keV μm^{-1} corresponds to $M_1 = 1.25$. From our measurements in propane gas we know that carbon ions with a LET of 100 keV μm^{-1} (approximately 225 MeV in kinetic energy) produce a mean ionisation yield $M_1 = 1.25$ if the gas density is adjusted to simulate a water target of about 1 nm in diameter and height. The equivalence of cluster size distributions measured in gaseous volumes of propane and in water volumes was discussed in (Grosswendt et al., 2004). In other words, if the nanodosimeter simulates a target site of the size equivalent to a water cylinder of 1 nm in diameter and height, the measured nanodosimetric quantity F_2 is directly proportional to the inactivation cross section of V79 cells at 5% survival level. The coefficient of proportionality, $C_{5\%} = 65$ μm^2, corresponds to the saturation of the inactivation cross section to the geometrical cross section of the V79 cell nuclei.

Other radio-resistant cell lines show a similar trend as the V79 cells, when analysed as a function of LET, and only saturate at different values. Consequently, we can expect that the same direct proportionality of F_2 to $\sigma_{5\%}$ also holds for other cells that are similar to the V79 cells from the point of view of their capability for DNA

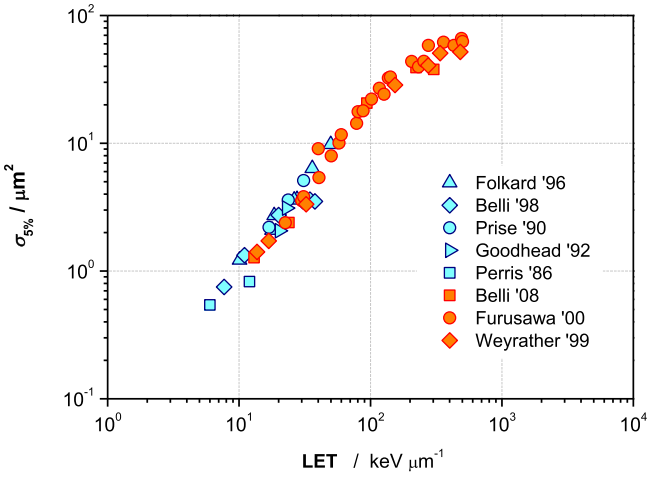

Fig. 3. Inactivation cross sections $\sigma_{5\%}$ for V79 cells irradiated by protons (light blue symbols) or carbon ions (orange symbols) against the LET of the incident particle.

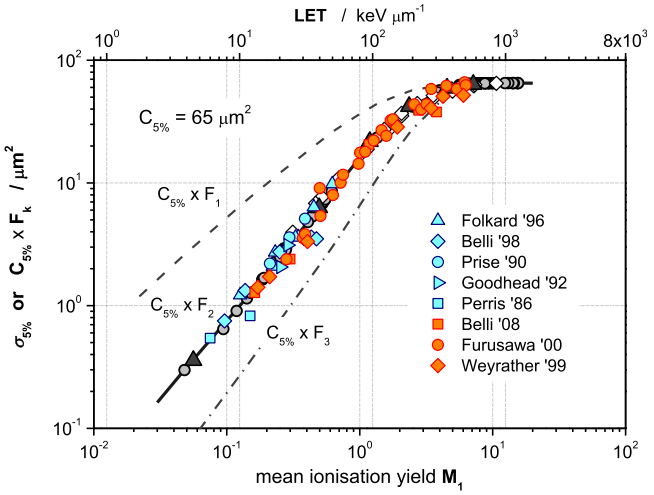

Fig. 4. The inactivation cross sections $\sigma_{5\%}$ for V79 cells of Fig. 3 (coloured symbols), as a function of *LET* (upper x-axis) and the scaled nanodosimetric $F_k(Q, V)$, for $k = 1, 2, 3$ (black and grey symbols and lines), as a function of the mean ionisation yield M_1 (lower x-axis).

repair (i.e. repair proficient), only with different coefficients of proportionality. This hypothesis was confirmed, among others, for Chinese hamster ovary (CHO) cells irradiated with carbon ions and for human submandibular gland (HSG) cells irradiated with helium and carbon ions, as shown in Fig. 5.

To investigate the correlation between nanodosimetric quantities and radiobiological data for different survival levels, the inactivation cross sections at low doses σ_α were also calculated from the initial slope of survival curves. Inactivation cross sections σ_α of V79 cells and the nanodosimetric quantities F_1, F_2 and F_3, multiplied by a constant proportionality coefficient $C_\alpha = 50\ \mu m^2$, are shown in Fig. 6; horizontal axes are chosen as in Fig. 4. At first glance there is an almost perfect overlap of the biological and the physical data F_3. In order to optimize this overlap, the upper horizontal axis has been shifted in such a way that LET = 100 keV μm^{-1} corresponds to $M_1 = 2$. From our measurements in propane gas we know that carbon ions with LET = 100 keV μm^{-1} produce a mean ionisation yield $M_1 = 2$ if the gas density is adjusted to simulate a water target of about 1.5 nm in diameter and height. In other words, if the nanodosimeter simulates a target site of the size equivalent to a water cylinder of 1.5 nm in diameter and height, the measured nanodosimetric quantity F_3 is directly proportional to the inactivation cross section of V79 cells at low doses.

To study the similarity between σ_α and F_3 also for other radioresistant cell lines, Fig. 7 shows the inactivation cross sections σ_α for HSG (Furusawa et al., 2000) and CHO cells (Czub et al., 2008; Mehnati et al., 2005; Scholz et al., 1997; Scholz, 2003; Weyrather et al., 1999). At first glance the proportionality to the physical quantity F_3 is confirmed, only with different coefficients C_α.

To analyse the behaviour of cells with different biological characteristics, the investigation was finally focused on XRS5, a radiosensitive genetic variant of CHO that shows an overall deficiency in DNA double strand break re-joining. Different from repair proficient cells, the XRS5 cells show a nearly straight survival curve, i.e. the cell survival fractions decrease exponentially with absorbed dose, so that in this case $\beta = 0\ Gy^{-2}$ and the inactivation cross section is the same at all survival levels. Since the repair capability is lower, it is expected that a rather simple damage at DNA level easily leads to a lethal effect.

The result of the comparison of the inactivation cross section of

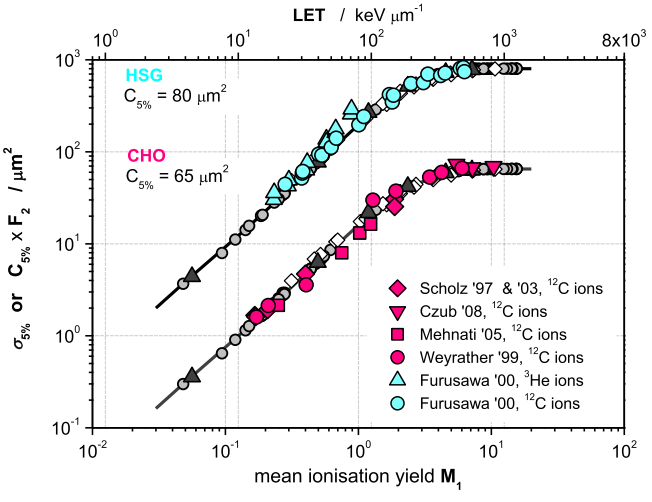

Fig. 5. The inactivation cross sections $\sigma_{5\%}$ for HSG (multiplied by 10) and CHO cells, as a function of *LET* (upper x-axis) and the scaled nanodosimetric $F_2(Q, V)$, as a function of the mean ionisation yield M_1 (lower x-axis). To facilitate the reading, the HSG data (and corresponding $C_{5\%}xF_2$) have been multiplied by 10. Coloured symbols represent biological data; grey symbols and solid line represent the physical experimental data.

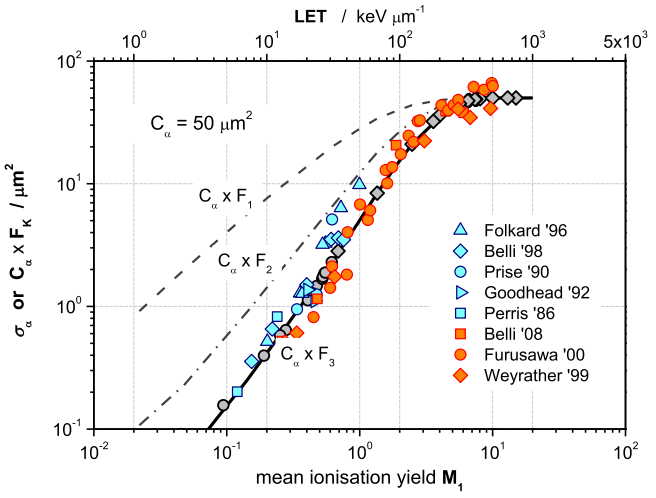

Fig. 6. The inactivation cross sections σ_α for V79 cells irradiated with protons and carbon ions, as a function of *LET* (upper x-axis) and the scaled nanodosimetric $F_k(Q, V)$, for $k = 1, 2, 3$, as a function of the mean ionisation yield M_1 (lower x-axis). Coloured symbols represent biological data; grey symbols and solid lines represent the physical experimental data.

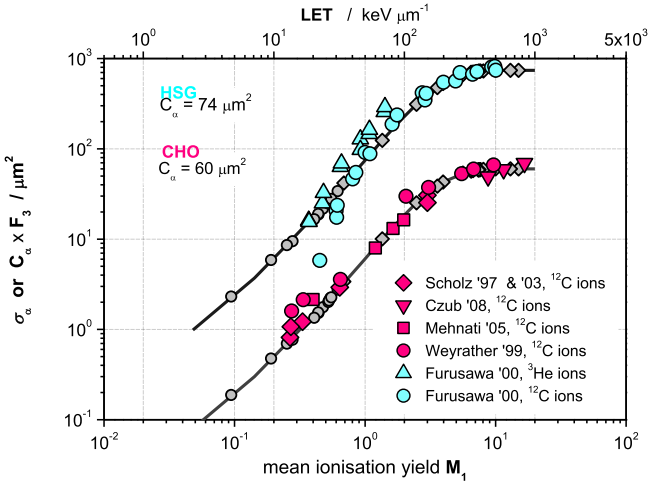

Fig. 7. The inactivation cross sections σ_α for HSG (multiplied by 10) and CHO cells, as a function of *LET* (upper x-axis) and the scaled nanodosimetric $F_3(Q, V)$, as a function of the mean ionisation yield M_1 (lower x-axis). To facilitate the reading, the HSG data (and corresponding $C_\alpha xF_3$) have been multiplied by 10. Coloured symbols represent biological data; the grey solid line represents the physical experimental data.

XRS5 cells (Weyrather et al., 1999) with the physical quantities F_1, F_2 and F_3, multiplied by a constant proportionality coefficient $C_\sigma = 190\ \mu m^2$, is shown in Fig. 8. At first glance Fig. 8 shows that the XRS5 cross sections are better modelled by F_1 rather than by F_2 or F_3. In order to optimize the correspondence between σ_{XRS5} and F_1, the upper horizontal axis has been shifted in such a way that the LET of 100 keV μm^{-1} corresponds to $M_1 = 0.3$. From our measurements in propane gas we know that carbon ions with a LET of 100 keV μm^{-1} produce a mean ionisation yield $M_1 = 0.3$ if the gas density is adjusted to simulate a water target of about 0.3 nm in diameter and height. In other words, if the nanodosimeter simulates a target site of the size equivalent to a water cylinder of 0.3 nm in diameter and height, the measured nanodosimetric quantity F_1 is directly proportional to the inactivation cross section of XRS5 cells at low doses. Since F_1 represents the probability of at least one

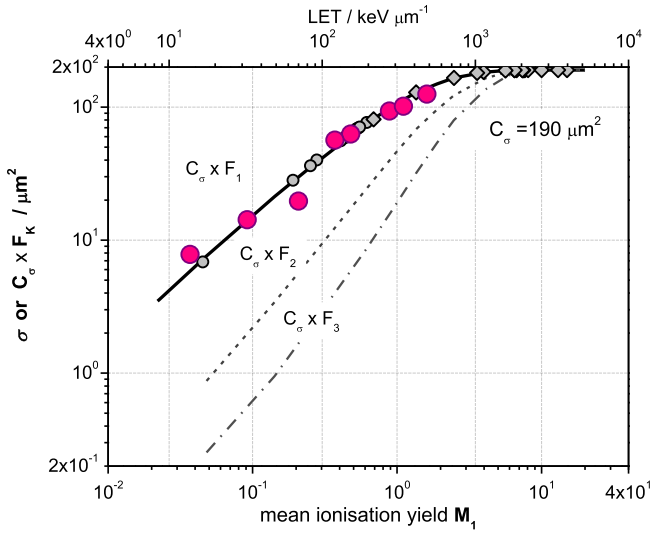

Fig. 8. The inactivation cross sections σ for XRS5 cells (symbols) as a function of particles' LET (upper x-axis), and the scaled nanodosimetric quantities $F_k(Q, V)$ (lines) as a function of the mean ionisation yield M_1 (lower x-axis). Coloured symbols represent biological data; the lines represent the physical experimental data.

ionisation, it corresponds to a DNA damage which is simpler than the damage produced for $k \geq 2$. The results shown in Fig. 8 can thus be explained in terms of the reduced repair capability of XRS5 cells.

4. Conclusions

An ionising particle of quality Q passing a nanometre-sized volume V produces ν ionisations inside V with probability $P_\nu(Q, V)$. Starting from measured distributions $P_\nu(Q, V)$ of the number of ionisations, the cumulative distribution function $F_k(Q, V)$ can be derived, which expresses the probability of measuring at least $\nu \geq k$ ionisations. Despite the different operating principles of the involved nanodosimeters and despite the different target sizes which were implemented, it was found that the measured cumulative probabilities $F_2(Q, V)$ lie on the same curve, when plotted versus the mean ionisation yield M_1. Furthermore, the curve $F_2(M_1)$ shows a saturation effect as M_1 increases beyond a certain threshold, which is similar to the behaviour of the inactivation cross sections with increasing LET. The same results were observed also for $F_1(M_1)$ and $F_3(M_1)$.

The analytical comparison between the cumulative probabilities F_k and the inactivation cross sections revealed a direct proportionality between the physical and the biological quantities. In more detail, it was found that (i) the inactivation cross section $\sigma_{5\%}$ for three lines of repair-proficient mammalian cells is proportional to the measurable nanodosimetric quantity F_2, that (ii) the inactivation cross section σ_α for the same cells is proportional to the measurable nanodosimetric quantity F_3, and that (iii) the inactivation cross section σ for repair-deficient XRS5 mammalian cells is proportional to the measurable nanodosimetric quantity F_1. For linear quadratic survival curves with $\beta \neq 0$ Gy^{-2}, the points (i) and (ii) suggest that after calibration of F_2 and F_3 with a specific radiation quality, measured F_2 and F_3 for unknown radiation quality can be used to predict initial survival, survival at 5% and also survival at any other level, by using F_2 and F_3 to calculate the α and β parameters of the linear quadratic model.

The direct proportionality of biological end points to physical quantities is anything but trivial, in particular if one considers the long time scale in which the action of ionising radiation evolves: regardless of the chemical and biochemical intermediate processes, there seems to be a direct link between the stochastics of ionisation in the early stage and the measurable biological effect in the later stage. Statistical moments of ionisation-cluster size distributions measured in nanometre-sized volumes could, therefore, lead to a new concept of radiation quality that builds on measurable physical properties of the radiation that are closely correlated with its potential to produce a biological damage. To validate the use of F_k to predict cell survival, a properly designed experiment with hypothesis testing is recommended.

Acknowledgements

This work was partially funded within the INFN Project MITRA, the EMRP Joint Research Project SIB06 BioQuaRT and under EC grant agreement 262010 (ENSAR). MITRA is funded by the 5th commission of INFN; the EMRP is jointly funded by the EMRP participating countries within EURAMET and the European Union.

References

Belli, M., Cera, F., Cherubini, R., Dalla Vecchia, M., Haque, A.M., Ianzini, F., Moschini, G., Sapora, O., Tabocchini, M.A., Tiveron, P., 1998. RBE–LET relationships for cell inactivation and mutation induced by low energy protons in V79 cells: further results at the LNL facility. Int. J. Radiat. Biol. 74, 501–509.

Belli, M., Bettega, D., Calzolari, P., Cherubini, R., Cuttone, G., Durante, M., Esposito, G., Furusawa, Y., Gerardi, S., Gialanella, G., Grossi, G., Manti, L., Marchesini, R., Pugliese, M., Scampoli, P., Simone, G., Sorrentino, E., Tabocchini, M.A., Tallone, L., 2008. Effectiveness of monoenergetic and spread–out Bragg peak carbon–ions for inactivation of various normal and tumour human cell lines. J. Radiat. Res. 49, 597–607.

Belloni, F., Bettega, D., Calzolari, P., Cherubini, R., Massariello, P., Tallone, L., 2002. Inactivation cross sections for mammalian cells exposed to charged particles: a phenomenological approach. Radiat. Prot. Dosim. 99 (1–4), 199–202.

Conte, V., Colautti, P., Grosswendt, B., Moro, D., De Nardo, L., 2012. Track structure of light ions: experiments and simulations. New J. Phys. 14, 093010.

Czub, J., Banaś, D., Błaszczyk, A., 2008. Biological effectiveness of 12C and 20Ne ions with very high LET. Int. J. Radiat. Biol. 84, 821–829.

Folkard, M., Prise, K.M., Voijnovic, B., 1996. Inactivation of V79 cells by low–energy protons, deuterons and helium–3 ions. Int. J. Radiat. Biol. 69, 729–738.

Furusawa, Y., Fukutsu, K., Aoki, M., Itsukaichi, H., Eguchi–Kasai, K., Ohara, H., Yatagai, F., Kanai, T., Ando, K., 2000. Inactivation of aerobic and hypoxic cells from three different cell lines by accelerated (3)He–, (12)C– and (20)Ne–ion beams. Radiat. Res. 154, 485–496.

Garty, G., Shchemelinin, S., Breskin, A., Chechik, R., Orion, I., Guedes, G.P., Schulte, R.W., Bashkirov, V.A., Grosswendt, B., 2002. Wall–less ion–counting nanodosimetry applied to protons. Radiat. Prot. Dosim. 99 (1–4), 325–330.

Goodhead, D.T., Belli, M., Mill, A.J., Bance, D.A., Allen, L.A., Hall, S.C., Ianzani, F., Simone, G., Stevens, D.L., Stretch, A., Tabocchini, M.A., Wilkinson, R.E., 1992. Direct comparison between protons and alpha particles of the same LET: I. Irradiation methods and inactivation of asynchronous V79, HeLa and C3H10T1/2 cells. Int. J. Radiat. Biol. 61, 611–624.

Grosswendt, B., De Nardo, L., Colautti, P., Pszona, S., Conte, V., Tornielli, G., 2004. Experimental equivalent cluster–size distributions in nanometric volumes of liquid water. Radiat. Prot. Dosim. 110, 851–857.

Mehnati, P., Morimoto, S., Yatagai, F., et al., 2005. Exploration of 'over kill effect' of high-LET Ar- and Fe-ions by evaluating the fraction of non-hit cell and inter-phase death. J. Radiat. Res. 46, 343–350.

Perris, A., Pialoglou, P., Katsanos, A.A., Sideris EG, E.G., 1986. Biological effectiveness of low energy protons. I. Survival of Chinese hamster cells. Int. J. Radiat. Biol. 50, 1093–1101.

Prise, K.M., Folkard, M., Davies, S., Michael, B.D., 1990. The irradiation of V79 mammalian cells by protons with energies below 2 MeV. Part II. Measurement of oxygen enhancement ratios and DNA damage. Int. J. Radiat. Biol. 58, 261–277.

Pszona, S., Kula, J., Marjanska, S., 2000. A new method for measuring ion clusters produced by charged particles in nanometre track sections of DNA size. Nucl. Instrum. Meth. A 447 (3), 601–607.

Pszona, S., Bantsar, A., Nikjoo, H., 2006. Ionization cluster size distribution for alpha particles: experiment, modelling. Radiat. Prot. Dosim. 122 (1–4), 28–31.

Scholz, M., Kellerer, A.M., Kraft-Weyrather, W., et al., 1997. Computation of cell survival in heavy ion beams for therapy. The model and its approximation. Radiat. Environ. Biophys. 1 (36), 59–66.

Scholz, M., 2003. Effects of ion radiation on cells and tissues. Adv Polym. Sci. 162, 95–155.

Weyrather, W.K., Ritter, S., Scholz, M., Kraft, G., 1999. RBE for carbon track–segment irradiation in cell lines of differing repair capacity. Int. J. Radiat. Biol. 75, 1357–1364.